An implicit RBF meshless approach for time fractional diffusion equations

Q. Liu[1]，Y. T. Gu[2*]，P. Zhuang[1], F. Liu[3], and Y.F. Nie[4]

1. *School of mathematical sciences, Xiamen University, 361005, Xiamen, China*

2. *School of Engineering Systems, Queensland University of Technology, Brisbane, Australia*

3. *School of Mathematical Sciences, Queensland University of Technology, Brisbane, Australia*

4. *School of Natural and Applied Sciences, Northwestern Polytechnical University, 710072, Xi'an China*

Abstract:

This paper aims to develop an implicit meshless approach based on the radial basis function (RBF) for numerical simulation of time fractional diffusion equations. The meshless RBF interpolation is firstly briefed. The discrete equations for two-dimensional time fractional diffusion equation (FDE) are obtained by using the meshless RBF shape functions and the strong-forms of the time FDE. The stability and convergence of this meshless approach are discussed and theoretically proven. Numerical examples with different problem domains and different nodal distributions are studied to validate and investigate accuracy and efficiency of the newly developed meshless approach. It has proven that the present meshless formulation is very effective for modeling and simulation of fractional differential equations.

Keywords: Fractional differential equation, Time fractional diffusion equation, Meshless method, Radial basis function, Implicit numerical scheme

1 Introduction

Many problems in engineering and sciences can be described by fractional ordinary differential equations (FODE) or fractional partial differential equations (FPDE). Recently, because of the new developments in sustainable environment and renewable energy, which are often governed by a series of FPDEs, the numerical modeling and

---

* Corresponding author: yuantong.gu@qut.edu.au

simulation for fractional calculus are attracting more and more attentions from research community [1][2][3]. It has become a new hot topic in computational mechanics and computational mathematics [4]. Fractional kinetic equations, such as fractional diffusion equation, fractional advection-diffusion equation, fractional Fokker-Planck equation, fractional cable equation etc., are recognized as useful approaches for the description of transport dynamics in complex systems including systems exhibiting Halmiltonian chaos, disordered medium, plasma and fluid turbulence, underground water pollution, dynamics of protein molecules, motions under the influence of optical tweezers, reactions in complex systems, and more [5]~[9]. When the fractional differential equations describe the asymptotic behaviour of continuous time random walks, their solutions correspond to the Lévy walks. The advantage of the fractional model for these problems basically lies in the straightforward way of including external force terms in calculating boundary value problems. Therefore, FPDE results in a more accurate representation of the relative phenomena than normal partial differential equations (PDEs).

Unlike the normal PDE, the differential order (regarding to time or space or both) in a FPDE is not with an integer order, in other words, with a fractional order (i.e., 0.5th order, 1.5th order, and so on), which will lead to a big difficulty in numerical simulation, because existing numerical simulation techniques are developed for PDE with an integer differential order. At present, most of FPDEs are solved numerically by Finite Difference Method (FDM) [10][11], when a few of research has been reported using Finite Element Method (FEM) [12][13][14]. FDM and FEM are numerical approaches based on pre-defined meshes/grids, which lead to inherited issues or shortcomings including: difficulty in handling a complex domain and irregular nodal distribution; difficulty in conducting adaptive analysis, and low computational accuracy. Therefore, these shortcomings become the main barrier for the development of a powerful simulation tool for practical applications governed by FPDE. The most current research in this field are still limited in some one-dimensional (1-D) or two-dimensional (2-D) benchmark problems with very simple domains (i.e., squares and rectangles) and Dirichlet boundary conditions.

Recent years, a group of meshless (or meshfree) methods have been developed and successfully used in many fields of computational mechanics [15]. Depending on whether a numerical integration is used in developing the system of algebraic

equations, the meshless methods can be largely grouped into two different categories [16]: meshless methods based on collocation techniques and meshless methods based on the general weak-forms of ordinary (partial) differential equations (ODEs or PDEs). The meshless methods based on collocation techniques, which can be developed by using Dirac- delta-test function, have a relatively long history, and they include smooth particle hydrodynamics (SPH) [17], the meshless collocation methods [18], finite point method (FPM) [19], etc. The so-called meshless methods, using various global weak-forms, were proposed about twenty years ago. This category of meshless methods includes the element-free Galerkin (EFG) method [20], the reproducing kernel particle method (RKPM)[21], and the point interpolation method (PIM) [22][23], the meshless local Petrov-Galerkin (MLPG) method [24], the local radial point interpolation method (LRPIM) [25][26], the boundary node method (BNM)[27], and the boundary point interpolation method (BPIM) [28][29].

The above discussed meshless methods have demonstrated distinguished advantages [15] including:

- They do not use a mesh (at least for field approximation), so that the burden of mesh generation in FDM and FEM is overcome. Hence, an adaptive analysis is easily achievable;

- They are usually more accurate than FDM and FEM due to the use of higher order meshless trial functions; and

- They are capable of solving complex problems that are difficult for the conventional FDM and FEM.

In spite of the impressive progresses, there are still some technical issues in the development of meshless techniques, for instance, a) the lack of theoretical study on the computational convergence and stability; b) the relatively worse computational efficiency; and c) the lack of commercial software packages for meshless analysis. Recently, some deep researches have been conducted and the above issues have been partially resolved [30][31]. Liu et al. proposed the formulation elaborated with a theoretical base on the G space theory [32]. Invoking the G space theory and the weakened weak-form (W2) [33], the meshless (or smoothed FEM) methods show a number of attractive properties, e.g., conformability, softness, upper/lower bound, super-convergence, ultra accuracy, and they also work well with triangular background cells. Another new development in meshless techniques is the

developments of the class of smoothed meshless methods, Smoothed Point Interpolation Method (S-PIM) and Smoothed FEM (S-FEM)[34]. However, this upper/lower bound property is obtained for the meshless methods based on weak-forms. Further study is still needed for the upper/lower bound property for meshfree techniques based on the strong-form, which we use in this paper.

Because of these unique advantages, meshless methods seem to have a good potential for the simulation of FPDE. Although the meshless methods have been successfully applied to a wide range of problems, for which, however, the governing equations are conventional PDE with an integer differential order, very limited work was reported to handle fractional partial differential equations (FPDE) by the meshless techniques. Chen et al.[35] used the Kansa method for fractional diffusion equations. Gu et al. [36] developed a meshless formulation for non-linear anomalous sub-diffusion equation. However, this topic still calls for a significant development.

The objective of this paper is to develop an implicit meshless formulation based on the radial basis functions (RBF) for numerical simulation of time fractional diffusion equation (FDE). The discrete equations for two-dimensional time fractional diffusion equation are obtained by using the meshless RBF shape functions and the strong-forms of time FDE. The essential boundary conditions are enforced by the direct collocation method [37]. The stability and convergence of the newly developed method are proven theoretically and numerically. Several numerical examples with different problem domains and different nodal distributions are used to validate and investigate accuracy and efficiency of the newly developed meshless formulation. Some important parameters of RBF are thoroughly investigated.

In this paper, we will develop a meshless collocation scheme using RBFs to spatially discretize the fractional convection-diffusion equation. We will also develop a higher order approximation for temporal discretization.

2 Time fractional diffusion equation

The time fractional diffusion equation can be written in the following form

$$\frac{\partial^{\alpha} u(\mathbf{x},t)}{\partial t^{\alpha}} = \kappa \Delta u(\mathbf{x},t) + f(\mathbf{x},t), \quad \mathbf{x} \in \Omega \subset \mathbf{R}^2, \quad t \in (0,T) \tag{1}$$

together with the general boundary and initial conditions

$$u(\mathbf{x},t) = g(\mathbf{x},t), \ \mathbf{x} \in \partial\Omega, \ t > 0 \tag{2}$$

$$u(\mathbf{x},0) = u_0(\mathbf{x}), \ \mathbf{x} \in \Omega \tag{3}$$

where Δ is the Laplace differential operator, Ω a bounded domain in $\mathbf{R}^2$, $\partial\Omega$ the boundary of Ω, κ the diffusion coefficient, T is the total time to be considered, $f(\mathbf{x},t)$, $g(\mathbf{x},t)$ and $u_0(\mathbf{x})$ are known functions.

In Equation (1), $\dfrac{\partial^\alpha u(\mathbf{x},t)}{\partial t^\alpha}$ is the Caputo fractional derivative of order $\alpha \ (0 < \alpha < 1)$ defined as

$$\frac{\partial^\alpha u(\mathbf{x},t)}{\partial t^\alpha} = \frac{1}{\Gamma(1-\alpha)} \int_0^t (t-\eta)^{-\alpha} \frac{\partial u(\mathbf{x},\eta)}{\partial \eta} \mathrm{d}\eta \tag{4}$$

2.1 Discretization of time

Define $t_k = k\Delta t$, $k = 1, 2, \cdots, n$, where $\Delta t = T/n$ is time step size. The time fractional derivative at $t = t_{k+1}$ can be approximated

$$\frac{\partial^\alpha u(\mathbf{x},t_{k+1})}{\partial t^\alpha} = \frac{1}{\Gamma(1-\alpha)} \sum_{j=0}^{k} \int_{t_j}^{t_{j+1}} (t_{k+1}-\eta)^{-\alpha} \frac{\partial u(\mathbf{x},\eta)}{\partial \eta} \mathrm{d}\eta \tag{5}$$

$$= \frac{1}{\Gamma(1-\alpha)} \sum_{j=0}^{k} \frac{u(\mathbf{x},t_{j+1})-u(\mathbf{x},t_j)}{\Delta t} \int_{t_j}^{t_{j+1}} (t_{k+1}-\eta)^{-\alpha} \mathrm{d}\eta + \tilde{R}_{k+1}$$

where the truncation error $\tilde{R}_{k+1}$ satisfies [38]

$$\left| \tilde{R}_{k+1} \right| \le C(\Delta t)^{2-\alpha} \tag{6}$$

Let $b_j = (j+1)^{1-\alpha} - j^{1-\alpha}$, $j = 0, 1, 2, \cdots, n$, then Equation (5) can be rewritten as

$$\frac{\partial^\alpha u(\mathbf{x},t_{k+1})}{\partial t^\alpha} = \frac{(\Delta t)^{-\alpha}}{\Gamma(2-\alpha)} \sum_{j=0}^{k} b_{k-j} \left[u(\mathbf{x},t_{j+1}) - u(\mathbf{x},t_j) \right] + \tilde{R}_{k+1} \tag{7}$$

or

$$\frac{\partial^{\alpha} u\left(\mathbf{x}, t_{k+1}\right)}{\partial t^{\alpha}}=\frac{(\Delta t)^{-\alpha}}{\Gamma(2-\alpha)} \sum_{j=0}^{k} b_{j}\left[u\left(\mathbf{x}, t_{k-j+1}\right)-u\left(\mathbf{x}, t_{k-j}\right)\right]+\tilde{R}_{k+1} \tag{8}$$

Substituting Equation (8) into Equation (1), we obtain

$$u\left(\mathbf{x}, t_{k+1}\right)-\mu_{1} \Delta u\left(\mathbf{x}, t_{k+1}\right) \tag{9}$$
$$=u\left(\mathbf{x}, t_{k}\right)-\sum_{j=1}^{k} b_{j}\left[u\left(\mathbf{x}, t_{k-j+1}\right)-u\left(\mathbf{x}, t_{k-j}\right)\right]+\mu_{2} f\left(\mathbf{x}, t_{k+1}\right)+R_{k+1}$$

where $\mu_{1}=\kappa(\Delta t)^{\alpha} \Gamma(2-\alpha)$, $\mu_{2}=(\Delta t)^{\alpha} \Gamma(2-\alpha)$ and

$$\left|R_{k+1}\right| \leq \tilde{C}(\Delta t)^{2} \tag{10}$$

where $\tilde{C}$ is a positive constant.

Let $u^{k}=u^{k}(\mathbf{x})$ be the numerical approximation to $u\left(\mathbf{x}, t_{k}\right)$ and $F^{k+1}=\mu_{2} f\left(\mathbf{x}, t_{k+1}\right)$, then Equations (1) - (3) can be discretized as the following scheme

$$u^{k+1}-\mu_{1} \Delta u^{k+1}=u^{k}-\sum_{j=1}^{k} b_{j}\left[u^{k+1-j}-u^{k-j}\right]+F^{k+1}, k=0,1, \cdots, n-1 \tag{11}$$

$$u^{0}=u_{0}(\mathbf{x}) \tag{12}$$

$$\left.u^{k}\right|_{\partial \Omega}=g\left(\mathbf{x}, t_{k}\right), k=0,1, \cdots, n \tag{13}$$

2.2 Stability and Convergence

In order to discuss the stability and convergence of Equations (11)-(13), let us introduce the following inner product

$$(v, w)=\iint_{\Omega} v(\mathbf{x}) w(\mathbf{x}) \mathrm{d}x \mathrm{d}y \tag{14}$$

and norm in L^{2}

$$\|v\|_{2}=[(v, v)]^{1/2}=\left[\iint_{\Omega} v^{2}(\mathbf{x}) \mathrm{d}x \mathrm{d}y\right]^{1/2} \tag{15}$$

The Equation (11) can be rewritten as

$$u^{k+1} - \mu_1 \Delta u^{k+1} = (1-b_1)u^k + \sum_{j=1}^{k-1}(b_j - b_{j+1})u^{k-j} + b_k u^0 + F^{k+1} \tag{16}$$

For this difference scheme, we have the following result.

Lemma 1 If $u^k(\mathbf{x}) \in H_0^2(\Omega)$, $k = 0,1,\cdots,n$ is the solution of Equation (11), then

$$\left\| u^k \right\|_2 \le \left\| u^0 \right\|_2 + b_{k-1}^{-1} \max_{0 \le l \le n} \left\| F^l \right\|_2 \tag{17}$$

Proof   We will prove the result by mathematical induction.

Firstly, when $k=0$, we have

$$u^1 - \mu_1 \Delta u^1 = u^0 + F^1 \tag{18}$$

By multiplying Equation (18) by u^1 and integrating on Ω, we obtain

$$\left\| u^1 \right\|_2^2 - \mu_1 \left(\Delta u^1, u^1 \right) = \left(u^0, u^1 \right) + \left(F^1, u^1 \right)$$

i.e.,

$$\left\| u^1 \right\|_2^2 + \mu_1 \left[\left(\frac{\partial u^1}{\partial x}, \frac{\partial u^1}{\partial x} \right) + \left(\frac{\partial u^1}{\partial y}, \frac{\partial u^1}{\partial y} \right) \right] = \left(u^0, u^1 \right) + \left(F^1, u^1 \right)$$

Using Schwarz inequality, we have

$$\left\| u^1 \right\|_2 \le \left\| u^0 \right\|_2 + \left\| F^1 \right\|_2 \le \left\| u^0 \right\|_2 + b_0^{-1} \max_{0 \le l \le n} \left\| F^l \right\|_2$$

Suppose now we have proven

$$\left\| u^j \right\|_2 \le \left\| u^0 \right\|_2 + b_0^{-1} \max_{0 \le l \le n} \left\| F^l \right\|_2, \quad j = 1, 2, \cdots, k \tag{19}$$

Multiplying Equation (16) by u^{k+1} and integrating on Ω, we obtain

$$\left\| u^{k+1} \right\|_2^2 - \mu_1 \left(\Delta u^{k+1}, u^{k+1} \right)$$
$$= (1-b_1)\left(u^k, u^{k+1} \right) + \sum_{j=1}^{k-1}(b_j - b_{j+1})\left(u^{k-j}, u^{k+1} \right) + b_k \left(u^0, u^{k+1} \right) + \left(F^{k+1}, u^{k+1} \right),$$

i.e.,

$$\left\|u^{k+1}\right\|_2^2 + \mu_1\left[\left(\frac{\partial u^{k+1}}{\partial x}, \frac{\partial u^{k+1}}{\partial x}\right) + \left(\frac{\partial u^{k+1}}{\partial y}, \frac{\partial u^{k+1}}{\partial y}\right)\right] \tag{20}$$

$$= (1-b_1)\left(u^k, u^{k+1}\right) + \sum_{j=1}^{k-1}\left(b_j - b_{j+1}\right)\left(u^{k-j}, u^{k+1}\right) + b_k\left(u^0, u^{k+1}\right) + \left(F^{k+1}, u^{k+1}\right)$$

Using Schwarz inequality, and the inequality [10]

$$b_j \geq b_{j+1}, \qquad j = 0, 1, \cdots, n,$$

we have

$$\left\|u^{k+1}\right\|_2 \leq (1-b_1)\left\|u^k\right\|_2 + \sum_{j=1}^{k-1}(b_j - b_{j+1})\left\|u^{k-j}\right\|_2 + b_k\left\|u^0\right\|_2 + \left\|F^{k+1}\right\|_2$$

Hence, by using Equation (19), we obtain

$$\left\|u^{k+1}\right\|_2 \leq \left\|u^0\right\|_2 + \left[\sum_{j=0}^{k-1}\left(b_j - b_{j+1}\right)b_{k-j-1}^{-1} + 1\right]\max_{0 \leq l \leq n}\left\|F^l\right\|_2$$

$$\leq \left\|u^0\right\|_2 + \left[\sum_{j=0}^{k-1}\left(b_j - b_{j+1}\right)b_k^{-1} + 1\right]\max_{0 \leq l \leq n}\left\|F^l\right\|_2 \tag{21}$$

$$\leq \left\|u^0\right\|_2 + b_k^{-1}\max_{0 \leq l \leq n}\left\|F^l\right\|_2 .$$

Suppose that $\tilde{u}^k(\mathbf{x})$, $k = 1, 2, \cdots, n$ is the solution of the Equation (16) with the initial condition $u(\mathbf{x}, 0) = \tilde{u}^0$ and the boundary condition Equation (13), then we have the following stability result.

Theorem 1 The fractional implicit numerical method defined by Equation (16) is un-conditionally stable.

Proof Denote the error

$$\varepsilon^k(\mathbf{x}) = u^k(\mathbf{x}) - \tilde{u}^k(\mathbf{x})$$

It satisfies

$$\varepsilon^{k+1} - \mu\Delta\varepsilon^{k+1} = (1-b_1)\varepsilon^k + \sum_{j=1}^{k}\left(b_j - b_{j+1}\right)\varepsilon^{k-j} + b_k\varepsilon^0$$

and

$$\varepsilon^{k+1}\big|_{\partial\Omega} = 0$$

From Lemma 1, we obtain

$$\left\|\varepsilon^k\right\|_2 \leq \left\|\varepsilon^0\right\|_2, \qquad k = 1, 2, \cdots, n \tag{22}$$

Now we carry out an error analysis for the solution of the time-discretized problem (16). We denote from now by c a generic constant which may not be the same at different occurrences.

Theorem 2 Let $\{u(\mathbf{x},t_k)\}_{k=0}^{n}$ be the exact solution of Equations (1)-(3), $\{u(\mathbf{x},t_k)\}_{k=0}^{n}$ be the time-discrete solution of Equation (16) with initial condition $u^0(\mathbf{x}) = u(\mathbf{x},0)$ and the boundary condition Equation (13), then we have the following error estimates

$$\left| u(\mathbf{x},t_k) - u^k(\mathbf{x}) \right| \le C(\Delta t)^{2-\alpha},$$

where C is a positive constant.

Proof Let $\xi^k(\mathbf{x}) = u(\mathbf{x},t_k) - u^k(\mathbf{x})$, from Equations (9) and (16), we obtain

$$\xi^{k+1}(\mathbf{x}) - \mu_1\Delta\xi^{k+1}(\mathbf{x}) = \xi^k(\mathbf{x}) - \sum_{j=1}^{k} b_j\left[\xi^{k+1-j}(\mathbf{x}) - \xi^{k-j}(\mathbf{x}) \right] + R_{k+1} \tag{23}$$

$$\xi^0(\mathbf{x}) = 0, \tag{24}$$

$$\xi^0(\mathbf{x})\big|_{\partial\Omega} = 0. \tag{25}$$

Hence, from Lemma 1, we have

$$\left\| \xi^k \right\|_2 \le b_{k-1}^{-1} \max_{0\le l\le n} \left\| R^l \right\|_2 \le C b_{k-1}^{-1} (\Delta t)^2 \tag{26}$$

Because $b_{k-1}^{-1}(\Delta t)^{\alpha}$ is bounded [10], thus

$$\left\| \xi^k \right\|_2 \le \tilde{C}(\Delta t)^{2-\alpha} \tag{27}$$

3 Construction of the meshless RBF shape function

At present, a number of ways to construct meshless shape functions have been proposed [15]. In this paper, the radial basis function (RBF) interpolation is used to construct the meshless shape functions for spatial discretization, because the RBF interpolation is stable and accurate [15]. The locally supported RBF interpolation formulation can be written as:

$$u(\mathbf{x}) = \sum_{i=1}^{n} R_i(r)a_i + \sum_{j=1}^{m} p_j(\mathbf{x})b_j = \mathbf{R}^T\mathbf{a} + \mathbf{B}^T\mathbf{b} = \{\mathbf{R} \quad \mathbf{B}\}\begin{Bmatrix} \mathbf{a} \\ \mathbf{b} \end{Bmatrix} \tag{28}$$

9

where $R_i(r)$ is the RBF, n is the number of nodes in the interpolation domain of point $\mathbf{x}$, $p_j(\mathbf{x})$ is a monomial in the space coordinates $\mathbf{x}^T = [x, y]$, m is the number of polynomial basis functions, and coefficients a_j and b_j are interpolation constants. The unique variable in a RBF is the distance, r, between the interpolation point $\mathbf{x}$ and a field node $\mathbf{x}_i$, and it makes the RBF interpolation easily extend to three-dimensional problems.

There is a number of RBFs, and their characteristics in meshless methods have been widely investigated [15]. In this paper, the following locally supported multiquadrics (MQ) RBF is used to construct the meshless shape function based on the local interpolation domains, which is written as

$$R_i(\mathbf{x}) = [r_i^2 + (\alpha_c d_i)^2]^q \tag{29}$$

where α_c is a dimensionless coefficient, and d_i is a parameter of the nodal spacing. The selections of two parameters (α_c and q) will significantly influence the performance of MQ RBF. The effects of α_c and q have been studied in details in many publications [15], and it was reported that $\alpha_c = 1.0$ and $q = 1.03$ lead to good results for most problems in computational mechanics. These two parameters will be also investigated in the following numerical studies.

It should be mentioned here that 'locally supported MQ RBF' means MQ RBF is employed to construct meshfree shape functions based on a local interpolation domain rather than the whole problem domain. In other words, for an interpolation point, only a small group of nodes, which are the closest to this interpolation point, are selected and used in the RBF interpolation [39].

Coefficients a_i and b_i in Equation (28) can be solved by enforcing Equation (28) to be satisfied at the n nodes surrounding a point $\mathbf{x}$. However, in Equation (28), there are only n equations for $n+m$ variables. To obtain unique solution, additional m equations should be added, which are the m constraint conditions, i.e.

$$\sum_{i=1}^{n} p_j(\mathbf{x}_i) a_i = \mathbf{B}_m^T \mathbf{a} = 0 \quad, \qquad j=1, 2, \ ..., \ m \tag{30}$$

Then, Equations (28) and (30) can be re-written in matrix form as follows

$$\begin{Bmatrix} \mathbf{u}_e \\ \mathbf{0} \end{Bmatrix} = \begin{bmatrix} \mathbf{R}_0 & \mathbf{B}_m \\ \mathbf{B}_m^{\mathrm{T}} & \mathbf{0} \end{bmatrix} \begin{Bmatrix} \mathbf{a} \\ \mathbf{b} \end{Bmatrix} = \mathbf{G}\mathbf{a}_0 \tag{31}$$

where u_e is the vector of nodal values for the field function of the nodes in the local interpolation domain.

$$\mathbf{R}_0 = \begin{bmatrix} R_1(r_1) & R_2(r_1) & \cdots & R_n(r_1) \\ R_1(r_2) & R_2(r_2) & \cdots & R_n(r_2) \\ \cdots & \cdots & \cdots & \cdots \\ R_1(r_n) & R_2(r_n) & \cdots & R_n(r_n) \end{bmatrix}$$

$$\mathbf{B}_m^{\mathrm{T}} = \begin{bmatrix} p_1(\mathbf{x}_1) & p_1(\mathbf{x}_2) & \cdots & p_1(\mathbf{x}_n) \\ p_2(\mathbf{x}_1) & p_2(\mathbf{x}_2) & \cdots & p_2(\mathbf{x}_n) \\ \vdots & \vdots & \ddots & \vdots \\ p_m(\mathbf{x}_1) & p_m(\mathbf{x}_2) & \cdots & p_m(\mathbf{x}_n) \end{bmatrix} \tag{32}$$

From Equation (30), coefficients $\mathbf{a}_0$ can be solved and substituting $\mathbf{a}_0$ back into Equation (28), the following RBF interpolation formulation is then obtained

$$\begin{aligned} u(\mathbf{x}) &= \{\mathbf{R} \quad \mathbf{B}\}\mathbf{G}^{-1} \begin{Bmatrix} \mathbf{u}_e \\ \mathbf{0} \end{Bmatrix} = \{\boldsymbol{\Phi}(\mathbf{x}) \quad \boldsymbol{\Lambda}(\mathbf{x})\} \begin{Bmatrix} \mathbf{u}_e \\ \mathbf{0} \end{Bmatrix} \\ &= \boldsymbol{\Phi}(\mathbf{x}) \cdot \mathbf{u}_e \end{aligned} \tag{33}$$

where the RBF shape function $\boldsymbol{\Phi}(\mathbf{x})$ is defined by

$$\boldsymbol{\Phi}(\mathbf{x}) = [\phi_1(\mathbf{x}), \phi_2(\mathbf{x}), \ldots, \phi_n(\mathbf{x})] = \left(\{\mathbf{R} \quad \mathbf{B}\}\mathbf{G}^{-1}\right)\Big|_{1-n} \tag{34}$$

where $\boldsymbol{\Phi}(\mathbf{x})$ is a vector which includes $1 \sim n$ elements of $(\mathbf{R} \quad \mathbf{B})\mathbf{G}^{-1}$ related to n nodes in the interpolation domain. The derivatives of $\boldsymbol{\Phi}(\mathbf{x})$ can be obtained

$$\frac{\partial \boldsymbol{\Phi}(\mathbf{x})}{\partial \mathbf{x}} = \left\{\frac{\partial \mathbf{R}}{\partial \mathbf{x}} \quad \frac{\partial \mathbf{B}}{\partial \mathbf{x}}\right\}\mathbf{G}^{-1} \tag{35}$$

$$\frac{\partial^2 \boldsymbol{\Phi}(\mathbf{x})}{\partial \mathbf{x}^2} = \left\{\frac{\partial^2 \mathbf{R}}{\partial \mathbf{x}^2} \quad \frac{\partial^2 \mathbf{B}}{\partial \mathbf{x}^2}\right\}\mathbf{G}^{-1} \tag{36}$$

It has been proven that the RBF shape functions given in Equation (33) satisfy the Kronecker delta condition [15], which makes it easy to enforce the Dirichlet boundary conditions in the meshless method based on the RBF shape functions.

11

4 Meshless approach

Consider the following fractional partial differential equation as presented in Equation (11)

$$u^{k+1} - \mu_1 \Delta u^{k+1} = u^k - \sum_{j=1}^{k} b_j \left[u^{k+1-j} - u^{k-j} \right] + F^{k+1}, \text{ in } \Omega \tag{37}$$

together with Dirichlet boundary condition

$$u^{k+1}(\mathbf{x}) = g(\mathbf{x}, t_{k+1}), \text{ on } \partial\Omega \tag{38}$$

Assume that there are N_d internal (domain) points and N_b boundary points. Hence, the following N_d equations at internal domain nodes can be obtained

$$\hat{u}^{k+1} - \mu_1 \Delta \hat{u}^{k+1} = \hat{u}^k - \sum_{j=1}^{k} b_j \left[\hat{u}^{k+1-j} - \hat{u}^{k-j} \right] + F^{k+1}, \text{ in } \Omega \tag{39}$$

The following N_b equations are satisfied on $\partial\Omega$

$$\hat{u}_i^{k+1} = g\left(\mathbf{x}_i, t_{k+1} \right), \quad i = 1, 2, \cdots, N_b. \tag{40}$$

Thus based on RBF interpolation, Equation (33), we have

$$\hat{u}^{k+1}(\mathbf{x}) = \sum_{i=1}^{n} \Phi_i \hat{u}_i^{k+1} \tag{41}$$

and its derivatives can be obtained by the following equations

$$\frac{\partial \hat{u}^{k+1}(\mathbf{x})}{\partial x} = \sum_{i=1}^{n} \frac{\partial \Phi_i}{\partial x} \hat{u}_i^{k+1} \tag{42}$$

$$\frac{\partial^2 \hat{u}^{k+1}(\mathbf{x})}{\partial x^2} = \sum_{i=1}^{n} \frac{\partial^2 \Phi_i}{\partial x^2} \hat{u}_i^{k+1} \tag{43}$$

$$\frac{\partial \hat{u}^{k+1}(\mathbf{x})}{\partial y} = \sum_{i=1}^{n} \frac{\partial \Phi_i}{\partial y} \hat{u}_i^{k+1} \tag{44}$$

$$\frac{\partial^2 \hat{u}^{k+1}(\mathbf{x})}{\partial y^2} = \sum_{i=1}^{n} \frac{\partial^2 \Phi_i}{\partial y^2} \hat{u}_i^{k+1} \tag{45}$$

where $\hat{u}$ means the field function for the point considered. Thus, $\hat{u}_i^{k+1}$ and its derivatives in Equation (39) can be obtained by substituting $\mathbf{x}$ into $\mathbf{x}_i$ in Equations (41) ~ (45)

$$\hat{u}_i^{k+1} = \hat{u}^{k+1}\left(\mathbf{x}_i\right), \quad \frac{\partial^2 \hat{u}_i^{k+1}}{\partial x^2} = \frac{\partial^2 \hat{u}^{k+1}\left(\mathbf{x}_i\right)}{\partial x^2}, \quad \frac{\partial^2 \hat{u}_i^{k+1}}{\partial y^2} = \frac{\partial^2 \hat{u}^{k+1}\left(\mathbf{x}_i\right)}{\partial y^2} \tag{46}$$

5 Numerical examples

In this section, some example cases are studied to demonstrate the effectiveness of the newly proposed meshless approach. In the following investigations, we will use the modified multiquadric RBF function as follows

$$R_i\left(r\right) = \left(r_i^2 + \left(\alpha_c d_c\right)^2\right)^q \tag{47}$$

where α_c and q are two shape parameters which have been thoroughly studied by Liu et al. [15]. In the first example, we investigate influences of different α_c and q. In equation (47), d_c is a characteristic length that is related to the nodal spacing in the local interpolation domain of the point of interest, which is defined in this paper as [39]: $d_c = \dfrac{\sqrt{S}}{\sqrt{S * N} - 1}$, where S means the area of the field Ω and N means the number of distributed field nodes.

We solve the following time fractional advection-diffusion equation

$$\frac{\partial^\alpha u(\mathbf{x},t)}{\partial t^\alpha} = \kappa \Delta u(\mathbf{x},t) + f(\mathbf{x},t), \quad \mathbf{x} \in \Omega \subset \mathbf{R}^2, \quad t \in (0,1) \tag{48}$$

$$u\left(\mathbf{x},t\right) = t^2 e^{x+y}, \quad \mathbf{x} \in \partial\Omega, \quad t \in (0,1) \tag{49}$$

$$u\left(\mathbf{x},0\right) = 0, \quad \mathbf{x} \in \Omega \tag{50}$$

where we employ $\kappa = 1.0$, and $f\left(\mathbf{x},t\right) = \left[\dfrac{2t^{2-\alpha}}{\Gamma\left(3-\alpha\right)} - 2t^2\right] e^{x+y}$.

The exact solution of Equations (48)-(50) is $u\left(\mathbf{x},t\right) = t^2 e^{x+y}$. As a fraction order in Equation (48), we take

$$\alpha = 0.85 \tag{51}$$

For quantitative studies, the following error notations are introduced

$$\varepsilon_{\max} = \max_i \left| u_i^{exact} - u_i^{num} \right|, \qquad \varepsilon_0 = \sqrt{\dfrac{\sum_{i=1}^{N} (u_i^{exact} - u_i^{num})^2}{\sum_{i=1}^{N} (u_i^{exact})^2}}, \tag{52}$$

$$\varepsilon_x = \sqrt{\dfrac{\sum_{i=1}^{N} (u_{i,x}^{exact} - u_{i,x}^{num})^2}{\sum_{i=1}^{N} (u_{i,x}^{exact})^2}}, \qquad \varepsilon_y = \sqrt{\dfrac{\sum_{i=1}^{N} (u_{i,y}^{exact} - u_{i,y}^{num})^2}{\sum_{i=1}^{N} (u_{i,y}^{exact})^2}} \tag{53}$$

where N denotes the number of all the grid nodes; u_i^{exact} and u_i^{num} are exact and numerical solutions, respectively, for interest point i; and $u_{i,}$ denotes the derivative.

5.1 A case with a rectangular problem domain

Firstly, we study a rectangular domain of $\Omega = [0,1] \times [0,1]$, which is discretized by $N = (n_x + 1) \times (n_y + 1)$ regularly distributed field nodes, as shown in Fig. 1 with $n_x = n_y = 40$. The newly proposed meshless method is used to simulate the time fractional diffusion equation with this rectangular problem domain.

Firstly the parameter of q is investigated. Figs. 2, 3 and 4 plot the computational errors for different q with $n_x = n_y = 10, 20, 30$, respectively. From Figs. 2, 3 and 4, it can be observed that $q = 1.03$ leads to better results than $q = 0.5$ and $q = 0.98$. It should be mentioned here that when $q = 0.5$, Equation (47) will become a standard multiquadric RBF function.

In addition, the influence of different α_c in Equation (47) has also been investigated. It has been found that although $\alpha_c = 3.4$ leads to better results, the computational accuracy is not sensitive for α_c. Hence, $q = 1.03$ and $\alpha_c = 3.4$ will be used in the following studies.

Fig. 5 plots the computational errors for different time steps. From this figure, it can be found, the error reduces with the decrease of time steps. In other words, a small time step leads to a more accurate result. We can also conclude from this figure that the present meshless method has good convergence. Table 1 listed the detailed results for computational errors, which have proven that the proposed meshless approach

14

achieved good computational accuracy. The convergence rates, R, of these four errors regarding to time steps are also listed in the same table. The convergent rate is calculated as:

$$R_\varepsilon = \frac{\varepsilon(\Delta t_1)}{\varepsilon(\Delta t_2)} \tag{54}$$

From Table 1, it can be seen that the convergence rates are close to

$$R_\varepsilon = \frac{\varepsilon(\Delta t_1)}{\varepsilon(\Delta t_2)} = \left(\frac{\Delta t_1}{\Delta t_2}\right)^{2-\alpha} = 2^{1.15} \approx 2.219. \tag{55}$$

It can be concluded that the order of convergences in time of the present method is $O(\Delta t^{2-\alpha})$. This is in good agreement with the results by the theoretical analysis.

For comparison, this problem has also been solved by the conventional Finite Difference Method (FDM), in which the regular grid as presented in Fig. 1 is used. It has been found that the newly developed meshless approach usually leads to better computational accuracy than FDM because the meshless RBF shape functions have better interpolation accuracy. However, meshless simulation needs more the computational cost than FDM. How to improve the computational efficiency for meshless techniques is still an open issue[15].

The irregularly distributed nodes, as shown in Fig. 6, are also used. The computational errors for different time steps are plotted in Fig. 7, in which the computational errors decrease with time steps. Table 2 listed the detailed results for computational errors. Comparing with results listed in Table 1, it can be found that the irregular nodal distribution leads to similar computational accuracy. It has proven that the proposed meshless approach achieved good computational accuracy for irregular nodes. The convergence rates, R, of these four errors regarding to time steps are also listed in Table 2. Using irregular nodes, the present meshless approach has good convergence rates which are close to those obtained by the regular nodes. Hence, the newly developed meshless technique is accurate and robust for not only the regular nodes but also the irregular nodes. It should mention here that the irregular grid will lead to a big difficulty for the conventional FDM.

5.2 A case with L-shaped problem domain

The $L-$shaped problem domain, given by the following equation and plotted in Fig. 8, is considered

$$\Omega = \left\{ (x, y) \middle| 0 \le x, y \le 1, sign(x-0.5) + sign(y-0.5) \le 0 \right\} \tag{56}$$

The regularly distributed nodes, as shown in Fig. 8, are firstly used to discretize this L-shaped problem domain. The computational errors for different time steps are plotted in Fig. 9 and listed in Table 3, which have proven that the proposed meshless approach performs very well for this case in terms of accuracy and convergence. The convergent rate is also in the order of $O(\Delta t^{2-\alpha})$.

The irregularly distributed nodes are also used for this problem with an L-shaped region, as shown in Fig. 10. The computational errors for different time steps are plotted in Fig. 11 and listed in Table 4. It can be concluded that the present meshless approach also leads to good computational accuracy and convergence rates for this L-shaped case using irregularly distributed nodes. It has proven the effectiveness of the meshless approach for a problem with a complex domain and irregular nodal distribution.

5.3 A case with a circular problem domain

Let us consider the following circular problem domain

$$\Omega = \left\{ (x, y) \middle| x^2 + y^2 \le 1 \right\}. \tag{57}$$

Total 1185 irregularly distributed nodes for this circular domain are used, as shown in Fig. 12. The computational errors are plotted in Fig. 13. It can be found that the developed meshless approach leads to accurate results.

5.4 A case with complex initial conditions

A rectangular domain $\Omega = [0,1] \times [0,1]$ is considered in this example, which investigates specifically the phenomenon of diffusion. The following initial and boundary conditions are considered:

$$u(\mathbf{x},0) = \begin{cases} x^{1.5} y^{1.5} & 0 < x \le 0.5, \ 0 < y < 0.5 \\ x^{r_1}(1-y)^{r_2} & 0 < x < 0.5, \ 0.5 < y < 1 \\ (1-x)^{r_1} y^{r_2} & 0.5 < x \le 1, \ 0 < y < 0.5 \\ (1-x)^{r_1}(1-y)^{r_2} & 0.5 < x < 1, \ 0.5 < y < 1 \end{cases} \tag{58}$$

$$u(\mathbf{x},t) = 0, \quad \mathbf{x} \in \partial\Omega, \ t > 0 \tag{59}$$

From Equation (58), we can find that this problem has complex initial conditions with four different segments. Therefore, there is no exact solution for this problem. The newly developed meshless approach is used to solve this time fractional advection-diffusion equation as given in Equation (48) together with Equations (58) and (59). The numerical simulation results of the diffusion process at different time are shown in Figs. 14, 15 and 16. From these figures, it can be found the newly developed meshless technique leads to smooth and stable results.

In summary, the above investigations have proven that the newly developed meshless approach is robust and has good accuracy and convergence rates even using irregular nodal distributions and/or for a complex domain. It should mention here that the irregularly nodal distribution and a non-rectangular problem domain will lead to big difficulty for the conventional Finite Difference Method.

6 Conclusions

This paper aims to develop an implicit meshless approach based on the radial basis function (RBF) for numerical simulation of time fractional diffusion equations (FDE), which is a type of fractional partial differential equation (FPDE). The stability and convergence of this meshless approach are then proven theoretically and numerically. Several numerical examples with different problem domains are used to study accuracy and efficiency of the newly developed meshless approach. Both regular and

irregular nodal distributions are employed in studies. From above studies, the following conclusions can be drawn:

- The shape parameters of MQ-RBF affect computational performance. $q = 1.03$ and $\alpha_c = 3.4$ are recommended for simulation of FDE;

- The convergence order of this present method regarding to time is $O(\Delta t^{2-\alpha})$;

- The presented meshless approach is un-conditionally stable;

- The newly developed meshless approach is accurate and convergent. Most importantly, the present approach is robust for arbitrarily distributed nodes and complex domains, for which the conventional Finite Difference Method (FDM) is difficult to handle.

In summary, the present meshless formulation is very effective for modeling and simulation of fractional differential equations, and it has good potential in development of a robust simulation tool for problems in engineering and science which are governed by the various types of fractional differential equations. In our future research, we will study more complicated problems.

References

[1] Agrawal O. P., Machado J. A. T. and Sabatier J., Introduction, Nonlinear Dynamics, 38 (2004), 1-2

[2] Butzer P. L. and Georges A., An Introduction to Fractional Calculus, World Scientific, Singapore, 2000

[3] Kenneth S. M. and Bertram R., An Introduction to the fractional calculus and fractional differential equations, Wiley-Interscience, New York, 1993.

[4] Zhou Y (ed.), Advance in Fractional Differential Equations. Computers and Mathematics with Applications 59(3) (2010), 1047-1376.

[5] Chechkin A., Gonchar V. Y., Kflafter J. and Metzler R., Fundamentals of Lévy fight processes, Advances in Chemical Physics, 133 (2006), 436-496

[6] Metzler R. and Klafter J., The random walk's guide to anomalous diffusion a fractional dynamics approach, Physics Reports, 339(1) (2000), 1-77

[7] Metzler R. and Klafter J., The restaurant at the end of the random walk: Recent developments in the description of anomalous transport by fractional dynamics. Journal of Physics A: Mathematical and General, 37(2) (2004), R161-R208

[8] Sokolov I., Klafter J. and Blumen A., Fractional kinetic equations, Physics Today, 55(2002), 48-54

[9] Zaslavsky G., Chao, fractional kinetics, and anomalous transport. Physics Reports, 371(1) (2002), 461-580

[10] Liu F., Zhuang P., Anh V., Turner I. and Burrage K., Stability and convergence of the difference methods for the space-time fractional advection-diffusion equation, Applied Mathematics and Computation, 191 (2007) , 12–20

[11] Meerschaert, M.and Tadjeran C.: Finite difference approximations for fractional advection-dispersion flow equations, Journal of computational and applied mathematics, 172 (2004), 65–77

[12] Ervin V. J. and Roop J. P., Variational formulation for the stationary fractional advection dispersion equation, Numerical Methods Partial Differential Equations, 22 (2005), 558-576

[13] Roop J. P., Computational aspect of FEM approximation of fractional advection dispersion equation on bounded domains in R2 , Journal of Computational and Applied Mathematics, 193(1) (2006), 243-268

[14] Ervin V. J., Heuer N. and Roop J. P., Numerical approximation of a time dependent, nonlinear, space-fractional diffusion equation, SIAM Journal of Numerical Analysis, 45(2007), 572-591

[15] Liu G. R. and Gu Y. T., An introduction to meshfree methods and their programming. Springer Press, Berlin, 2005

[16]Gu Y.T., Meshfree methods and their comparisons. International Journal of Computational Methods, 2 (4) (2005), 477-515.

[17] Gingold R. A. and Moraghan J. J., Smooth particle hydrodynamics: theory and applications to non spherical stars. Monthly Notices of the Royal Astronomical Society, 181 (1977), 375-389

[18] Kansa E. J.: Multiquadrics-A Scattered Data Approximation Scheme with Applications to Computational Fluid dynamics. Computers Math. Applic., 19(8/9) (1990), 127–145

[19] Onate E., Idelsohn S., Zienkiewicz O. C., Taylor R. L. and Sacco C., A finite method in computational mechanics: applications to convective transport and fluid flow, International Journal of Numerical Methods in Engineering, 39 (1996), 3839-3866

[20] Belytschko T., Lu Y. Y. and Gu L., Element-Free Galerkin Methods. International Journal for Numerical Methods in Engineering, 37 (1994), 229-256

[21] Liu W. K., Jun S., Zhang Y., Reproducing kernel particle methods. International Journal for Numerical Methods in Engineering, 20 (1995), 1081-1106

[22] Liu G. R. and Gu Y. T., A point interpolation method for two-dimensional solids. International Journal for Numerical Methods in Engineering, 50 (4) (2001), 937-951

[23]Liu G.R. and Gu Y.T., Assessment and applications of point interpolation methods for computational mechanics. International Journal for Numerical Methods in engineering, 59(10) (2004), 1373-1397.

[24] Atluri S. N. and Zhu T., A new meshfree local Petrov-Galerkin (MLPG) approach in computational mechanics. Computational Mechanics, 22 (1998), 117-127

[25] Liu G. R. and Gu Y. T., A local radial point interpolation method (LR-PIM) for free vibration analyses of 2-D solids. Journal of Sound and Vibration, 246(1) (2001), 29-46

[26]Liu G.R. and Gu Y.T., Comparisons of two meshfree local point interpolation methods for structural analyses, Computational Mechanics, 29(2) (2002), 107-121.

[27] Mukherjee Y. X. and Mukherjee S., Boundary node method for potential problems. Int. J. Num. Methods in Engrg., 40 (1997), 797-815

[28] Gu Y. T. and Liu G. R., A boundary point interpolation method for stress analysis of solids. Computational Mechanics, 28 (2002), 47-54

[29] Gu Y. T. and Liu G. R., A boundary radial point interpolation method (BRPIM) for 2-D structural analyses. Structural Engineering and Mechanics, 15 (5) (2003), 535-550

[30] Liu G. R. and Zhang G. Y., Upper bound solution to elasticity problems: A unique property of the linearly conforming point interpolation method (LC-PIM). International Journal for Numerical Methods in Engineering, 74 (2008), 1128–1161

[31] Liu G. R., Gu Y. T. and Dai K. Y., Assessment and applications of point interpolation methods for computational mechanics. International Journal for Numerical Methods in Engineering, 59 (10) (2004), 1373-1397

[32] Liu G. R., On G space theory. International Journal of Computational Methods, 6(2) (2009), 257–289

[33] Liu G. R., A G space and weakened weak (W2) form for a unified formulation of compatible and incompatible methods, part I–Theory and part II–Application to solid mechanics problems, International Journal for Numerical Methods in Engineering, 2008

[34] Liu G. R., Dai K. Y. and Nguyen T. T., A smoothed finite element method for mechanics problems. Computational Mechanics, 39 (2007), 859–877.

[35] Chen, W.; Ye, L.; Sun, H., Fractional diffusion equations by the Kansa method. Computers and Mathematics with Applications, 59(5) (2010), 1614-1620.

[36] Gu Y.T., Zhuang P.H. and Liu F.W., An advanced implicit meshless approach for the non-linear anomalous subdiffusion equation. CMES-Computer Modeling in Engineering & Sciences, 56 (3) (2010), 303-333.

[37] Zhu T. and Atluri S. N., A Modified collocation method and a penalty formulation for enforcing the essential boundary conditions in the element free Galerkin method, Computational Mechanics, 21 (1998), 211-222

[38] Yumin Lin and Chuanju Xu, Finite difference/spectral approximations for the time-fractional diffusion equation, J. Comp. Phys., 225(2) (2007), 1533-1552.

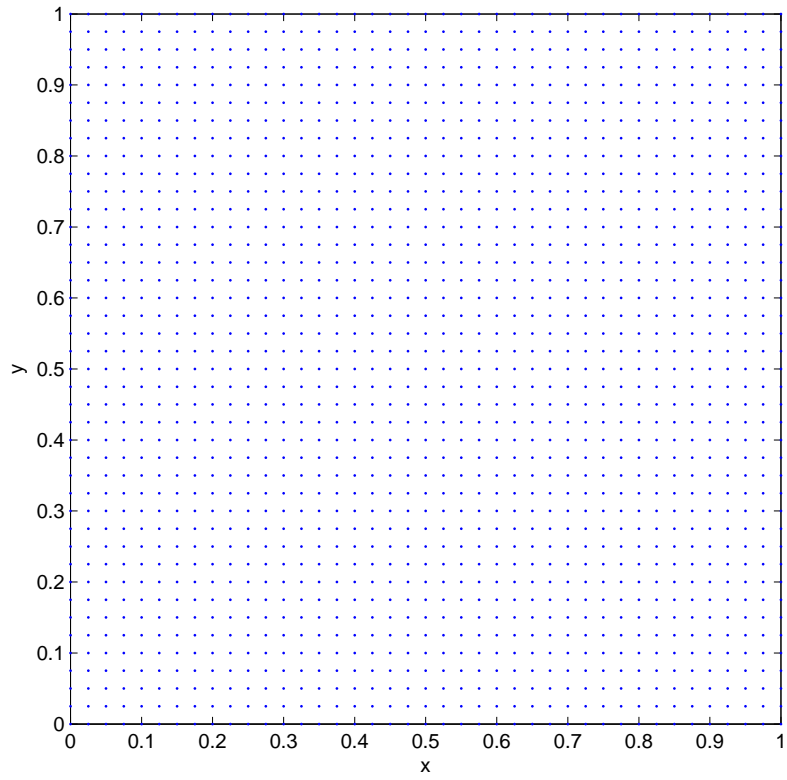[39] Liu G.R., Mesh Free Methods: Moving Beyond the Finite Element Method (2nd Edition). CRC press, USA, 2009

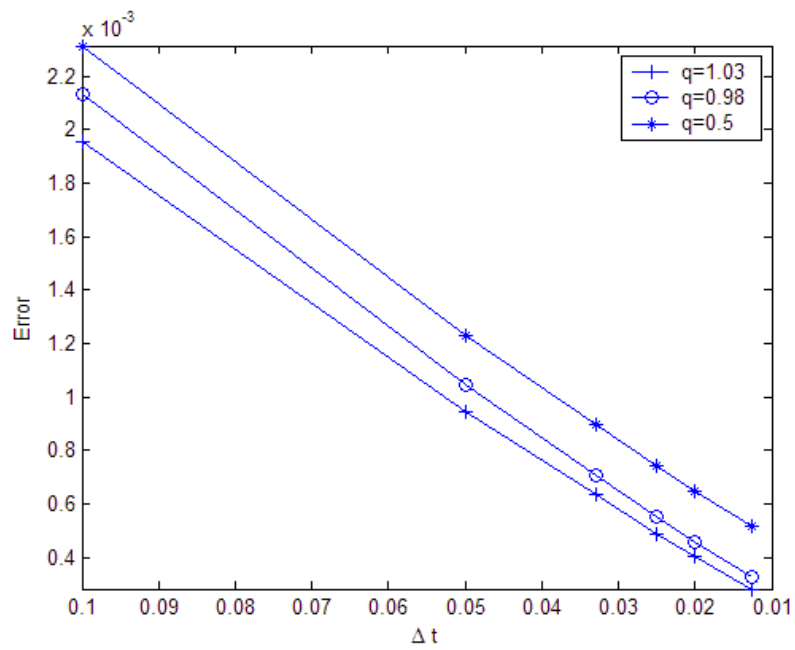Figure 1: Regular distribution of points on rectangular domain

.

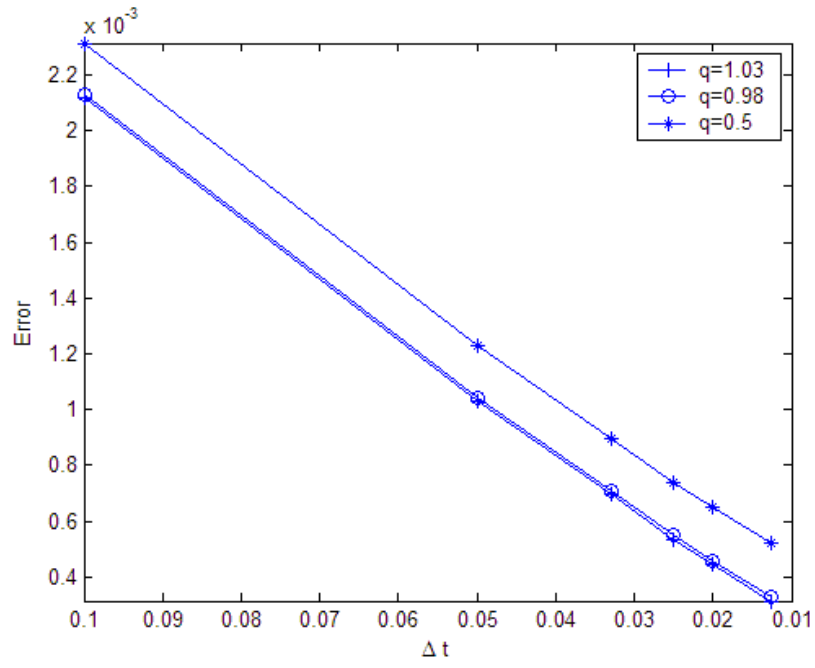Figure 2: Influence of parameter q with $n_x = n_y = 10$

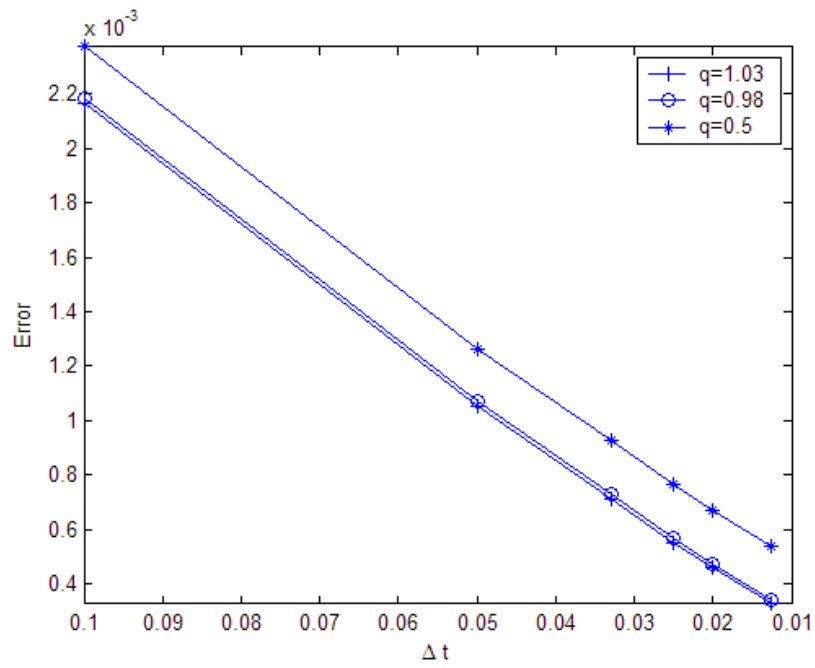Figure 3: Influence of parameter q with $n_x = n_y = 20$

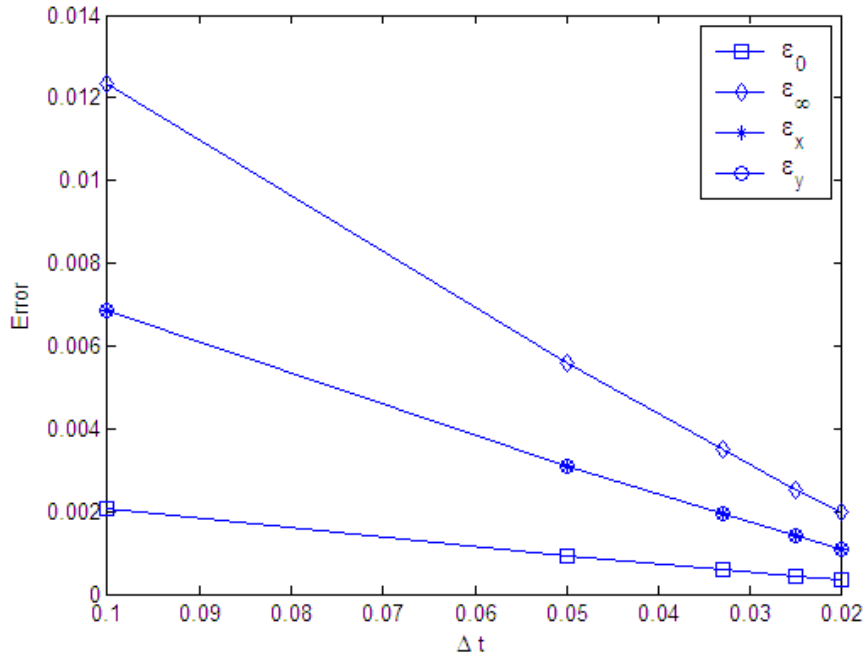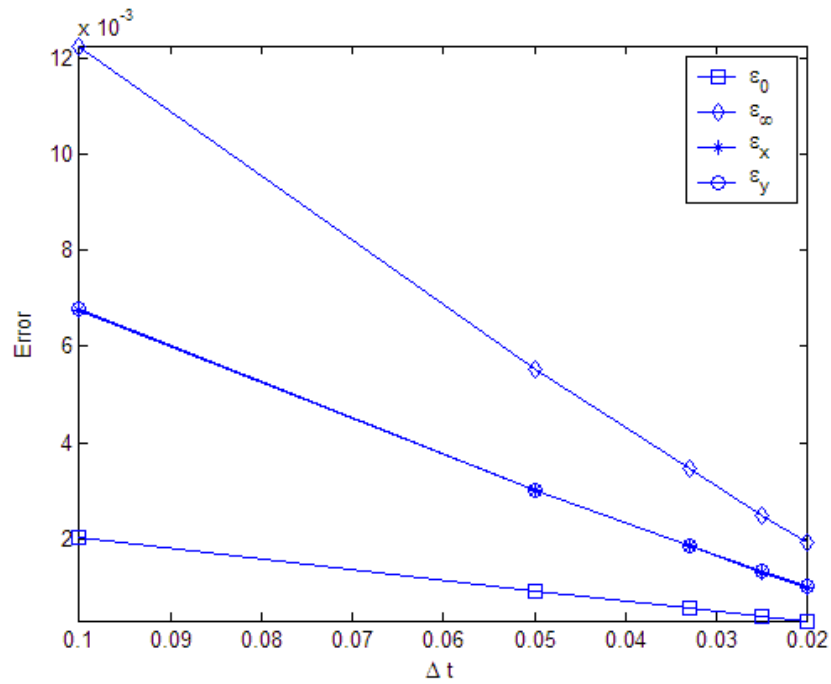Figure 4: Influence of parameter q with $n_x = n_y = 30$

22

Figure 5: Errors as a function of the time step Δt (Regular nodal distribution on rectangular region)

Table1: The error obtained using meshless approach at $t = 1.0$ (Regular nodal distribution on rectangular region)

Δt	ε_{max}	$R_{\varepsilon max}$	ε_0	$R_{\varepsilon 0}$	ε_x	$R_{\varepsilon x}$	ε_y	$R_{\varepsilon y}$
0.1	1.234e-2	---	2.073e-3	---	6.864e-3	---	6.864e-3	---
0.05	5.578e-3	2.212	9.370e-4	2.212	3.103e-3	2.212	3.103e-3	2.212
0.025	2.520e-3	2.213	4.234e-4	2.213	1.402e-3	2.213	1.402e-3	2.213
0.0125	1.140e-3	2.211	1.916e-4	2.210	6.345e-4	2.210	6.345e-4	2.210
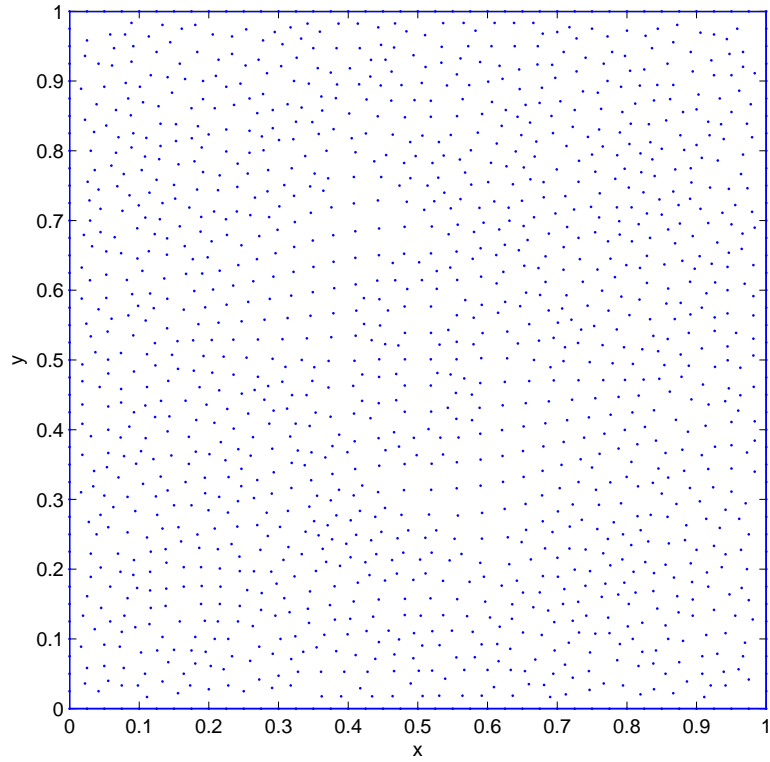
Figure 6: Irregular distribution of points on rectangular domain

Figure 7: Errors as a function of the time step Δt (Irregular nodal distribution on rectangular region)

Table2: The error obtained using meshless approach at $t = 1.0$ (Irregular nodal distribution on rectangular region)

Δt	ε_{max}	$R_{\varepsilon max}$	ε_0	$R_{\varepsilon 0}$	ε_x	$R_{\varepsilon x}$	ε_y	$R_{\varepsilon y}$

0.1	1.225e-2	---	2.022e-3	---	6.751e-3	---	6.784e-3	---
0.05	5.516e-3	2.221	9.014e-4	2.243	3.003e-3	2.248	3.016e-3	2.249
0.025	2.488e-3	2.217	3.946e-4	2.284	1.312e-4	2.289	1.317e-3	2.290
0.0125	1.134e-3	2.192	1.660e-4	2.377	5.566e-4	2.357	5.608e-4	2.348
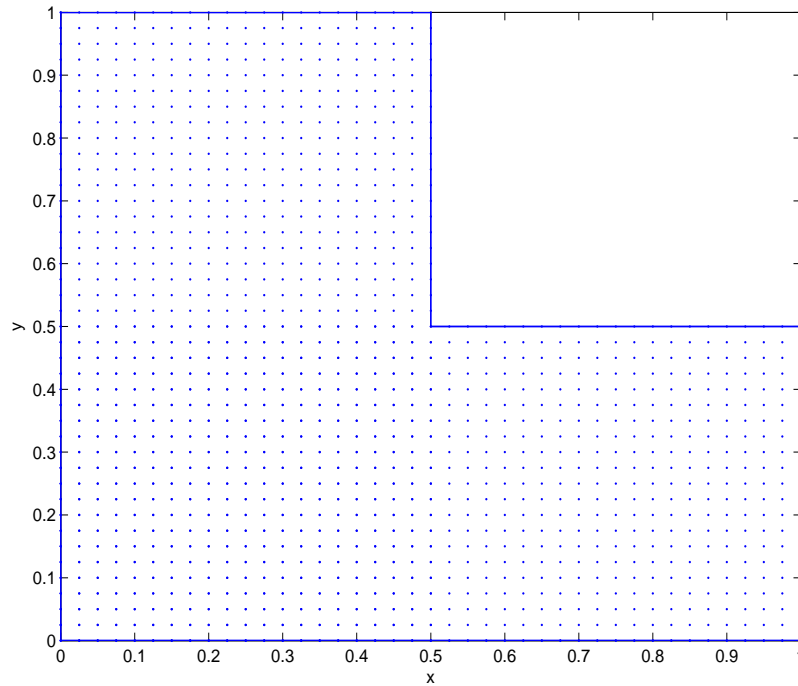
Figure 8: Regular distribution of points on *L*-shaped domain

Table3: The computational error obtained using meshless approach at *t* = 1.0 (Regular nodal distribution on *L*-shaped region)

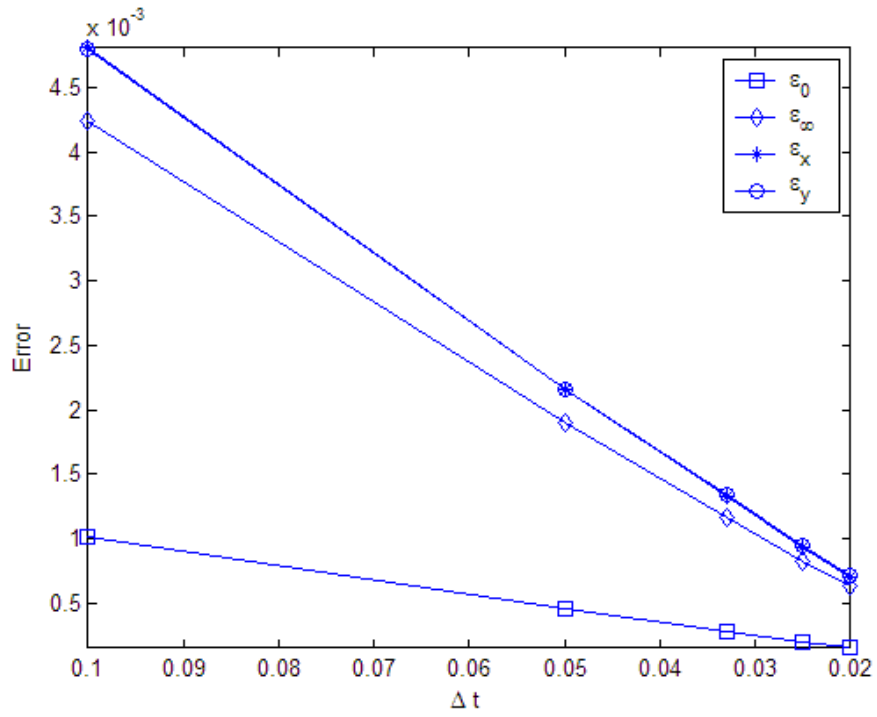| Δt	ε_{max}	$R_{\varepsilon max}$	ε_0	$R_{\varepsilon 0}$	ε_x	$R_{\varepsilon x}$	ε_y	$R_{\varepsilon y}$
0.1	4.351e-3	---	1.022e-3	---	4.856e-3	---	4.856e-3	---
0.05	1.967e-3	2.212	4.619e-4	2.213	2.195e-3	2.212	2.195e-3	2.212
0.025	8.888e-4	2.213	2.088e-4	2.212	9.919e-4	2.213	9.919e-4	2.213
0.0125	4.024e-4	2.209	9.451e-5	2.209	4.489e-4	2.210	4.489e-4	2.210

Figure 9: Errors as a function of the time step Δt (Regular nodal distribution on L-shaped region)
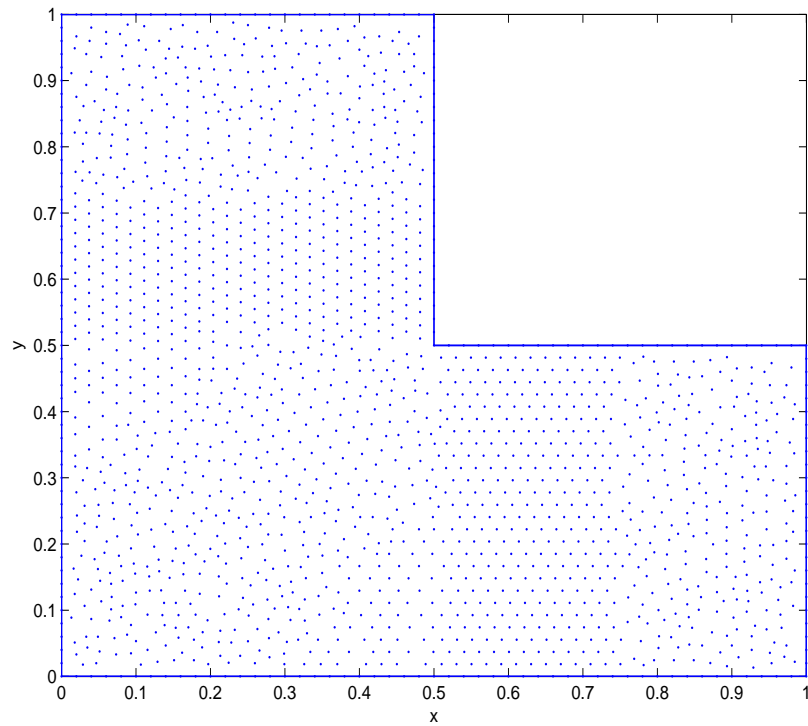

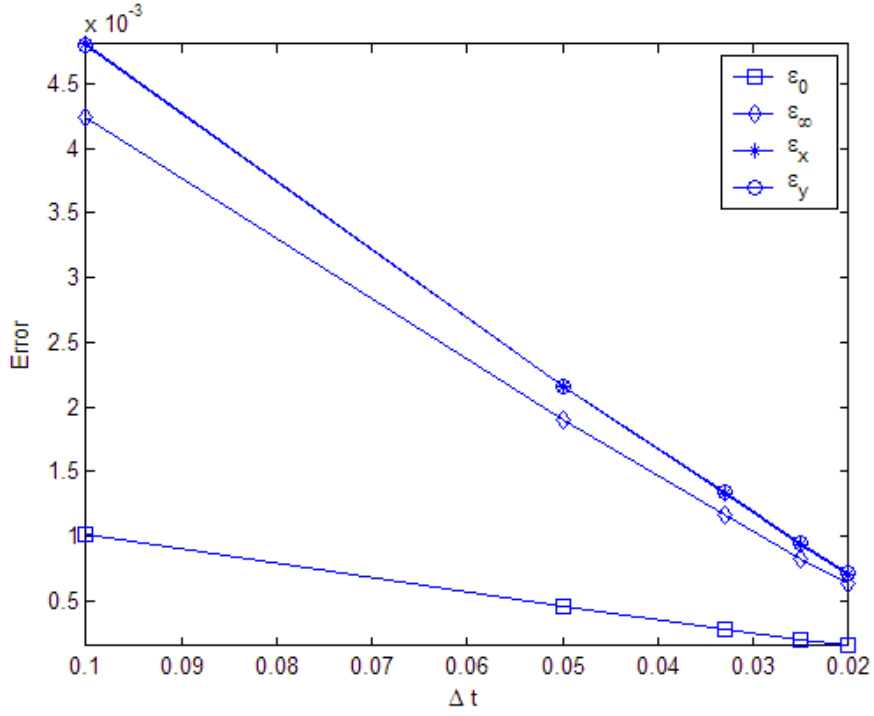Figure 10: Irregular distribution of points on L-shaped domain

26

Figure 11: Errors as a function of the time step Δt (Irregular nodal distribution on L-shaped region)

Table4: The error obtained using meshless approach at $t = 1.0$ (Irregular nodal distribution on $L-$shaped region)

Δt	ε_{max}	$R_{\varepsilon max}$	ε_0	$R_{\varepsilon 0}$	ε_x	$R_{\varepsilon x}$	ε_y	$R_{\varepsilon y}$
0.1	4.242e-3	---	1.010e-3	---	4.805e-3	---	4.792e-3	---
0.05	1.900e-3	2.233	4.544e-4	2.223	2.152e-3	2.233	2.157e-3	2.222
0.025	8.266e-4	2.299	1.992e-4	2.281	9.354e-4	2.301	9.460e-4	2.280
0.0125	3.606e-4	2.292	8.412e-5	2.368	3.887e-4	2.406	4.019e-4	2.353

27
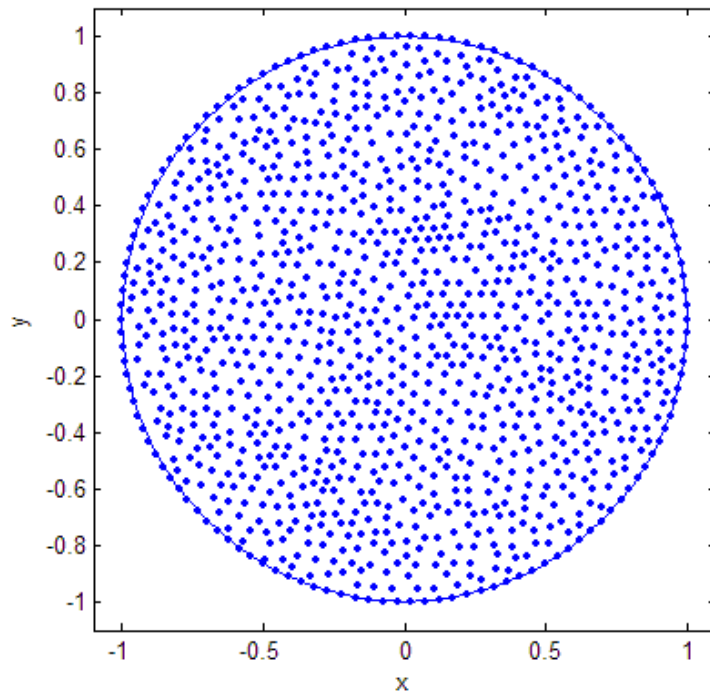
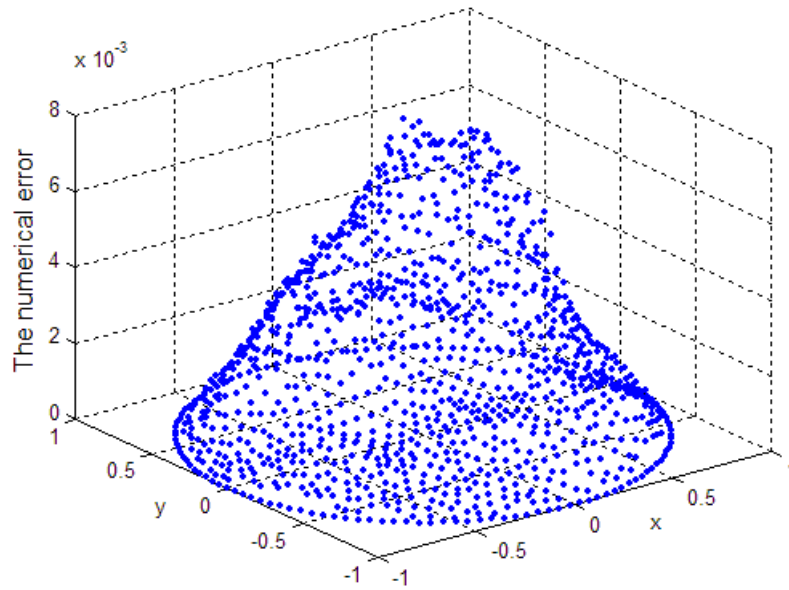Figure 12. Scattered distribution of points on circular domain

Figure 13: The error distribution at $t = 1.0$ (Irregular nodal distribution on circular domain)
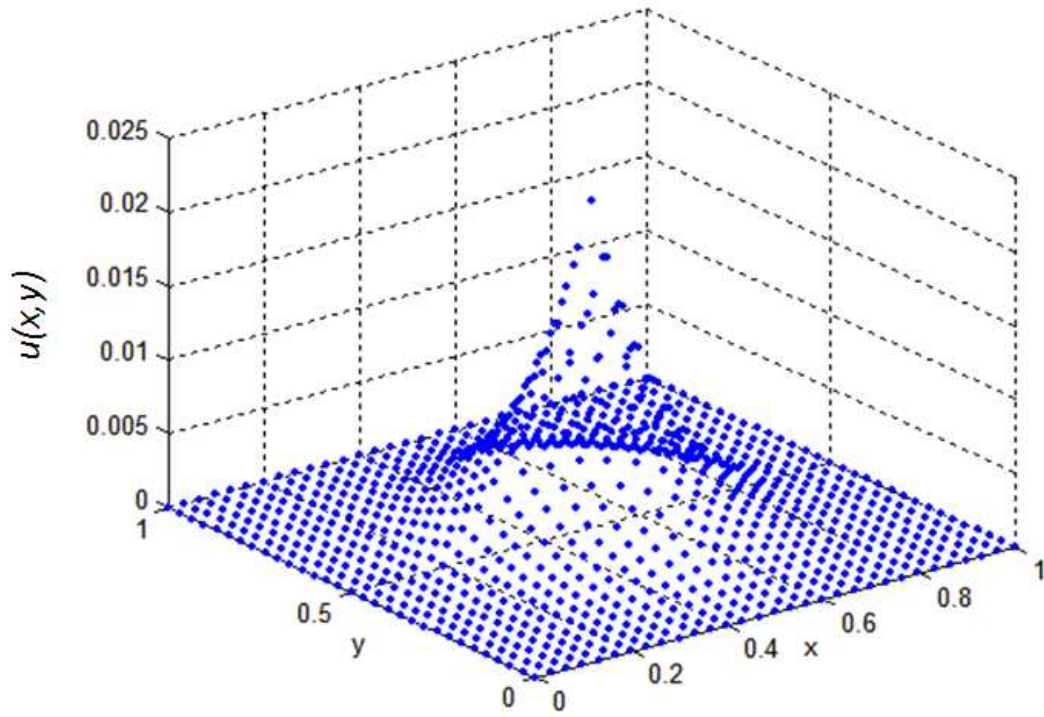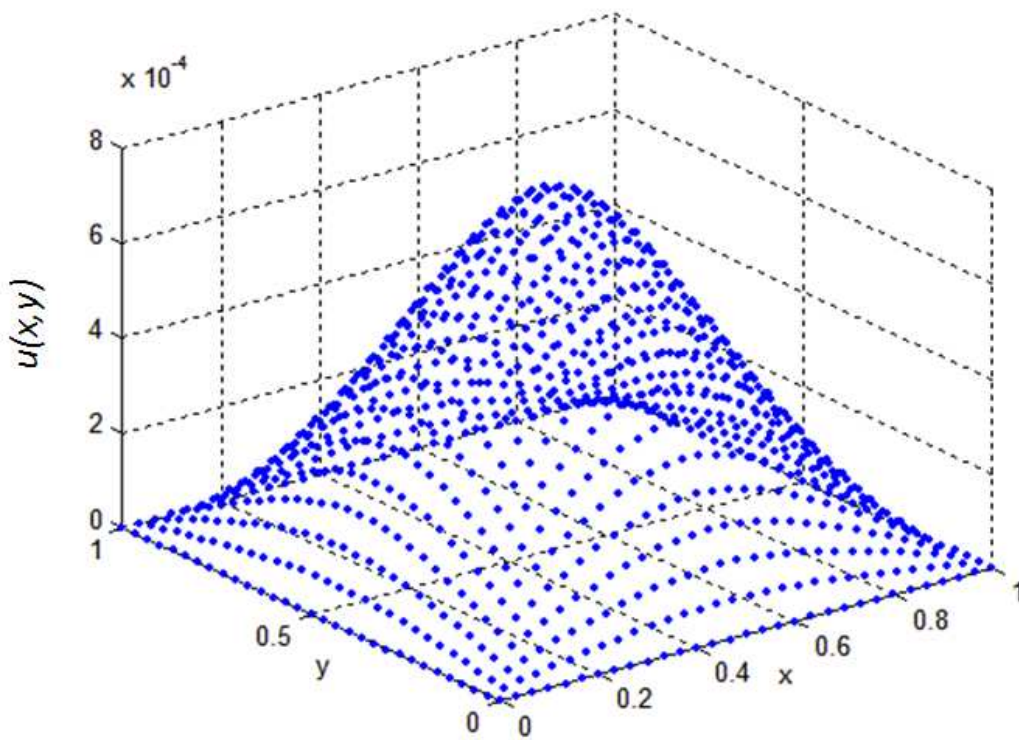
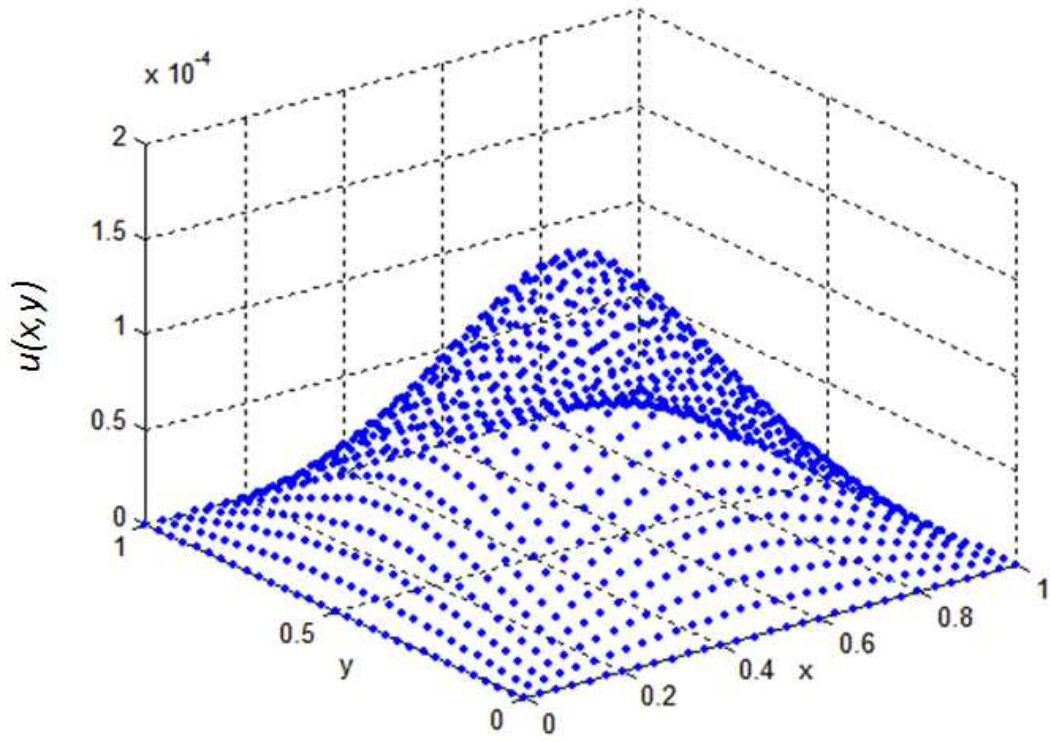Figure 14: The initial condition at $t = 0$

Figure 15: The numerical solution at $t = 0.1$

Figure 16: The numerical solution at $t = 0.4$